

Soil arching analysis in embankments on soft clays reinforced by stone columns

Mohammed Y. Fattah^{*1}, Bushra S. Zabar² and Hanan A. Hassan³

¹Building and Construction Engineering Department, University of Technology, Baghdad, Iraq

²Civil Engineering Department, University of Baghdad, Iraq

³Highway and Transportation Engineering Department, University of Al-Mustansiriya, Baghdad, Iraq

(Received March 20, 2015, Revised October 26, 2015, Accepted October 28, 2015)

Abstract. The present work investigates the behavior of the embankment models resting on soft soil reinforced with ordinary and stone columns encased with geogrid. Model tests were performed with different spacing distances between stone columns and two lengths to diameter ratios (L/d) of the stone columns, in addition to different embankment heights.

A total number of 42 model tests were carried out on a soil with undrained shear strength ≈ 10 kPa. The models consist of stone columns embankment at s/d equal to 2.5, 3 and 4 with L/d ratio equal 5 and 8. Three embankment heights; 200 mm, 250 mm and 300 mm were tested for both tests of ordinary (OSC) and geogrid encased stone columns (ESC).

Three earth pressure cells were used to measure directly the vertical effective stress on column at the top of the middle stone column under the center line of embankment and on the edge stone column for all models while the third cell was placed at the base of embankment between two columns to measure the vertical effective stress in soft soil directly.

The performance of stone columns embankments relies upon the ability of the granular embankment material to arch over the 'gaps' between the stone columns spacing. The results showed that the ratio of the embankment height to the clear spacing between columns ($h/s-d$) is a key parameter. It is found that $(h/s-d) < 1.2$ and 1.4 for OSC and ESC, respectively; (h is the embankment height, s is the spacing between columns and d is the diameter of stone columns), no effect of arching is pronounced, the settlement at the surface of the embankment is very large, and the stress acting on the subsoil is virtually unmodified from the nominal overburden stress. When $(h/s-d) \geq 2.2$ for OSC and ESC respectively, full arching will occur and minimum stress on subsoil between stone columns will act, so the range of critical embankment height will be $1.2 (h/s-d)$ to $2.2 (h/s-d)$ for both OSC and ESC models.

Keywords: embankment; soft clay; stone column; arching

1. Introduction

The increasing need for infrastructure development has often forced engineers to deal with

*Corresponding author, Professor, E-mail: myf_1968@yahoo.com

^aE-mail: albusoda@yahoo.com

^bE-mail: ghassan_hanan@yahoo.com

building on soft soils. The soft soil cannot take external load without having large deformations. Most of the construction methods techniques used to stabilize soft soil such as consolidation, low weight fill materials, over excavating of soft soil and replacement with fill material may be an expensive technique. One soil improvement technique is a “piled embankment”. In many cases, this method appears to be the most practical, efficient (low cost for long term cost and short construction time) and an environmentally-friendly solution for construction on soft soil.

The field applications are mainly highways, railways and construction of areas of fill for industrial or residential purposes. Piles are installed through the soft subsoil and transfer load to a more competent stratum at greater depth when the soft clay layer is thick; it is often that the piles cannot reach the competent stratum. These are called floating piles. Many types of non-deformable columns can be considered as piles for soft soil improvement such as timber piles, prefabricated or cast-in situ concrete piles, deep mixing lime cement columns, as well as grouted stone columns.

The majority of the load from the embankment is carried by the piles and thus there is relatively little load on the soft subsoil. By using a piled embankment, the construction can be undertaken in a single stage without having to wait for the soft clay to consolidate. Total and differential settlements are also significantly reduced when the technique is used successfully. Piles are typically arranged in square or triangular patterns in practice (Yan 2009).

In recent years, geosynthetics have been used in combination with pile or column system to support embankment over soft clay foundations (Han and Collin 2005). If geosynthetic layers are often included for the embankment reinforcement is laid on top of a thin layer of embankment material. It is not usually laid directly on top of pile caps. The application of geosynthetic(s) in the fill just above the pile, enhances the load transfer efficiency, minimizes yielding of soil above pile, and reduces the total and differential settlement (Han and Gabr 2002).

A series of twelve 3D laboratory model tests was performed on piled embankments by van Eekelen *et al.* (2012a). In this first part of a two-part study, the measured load distribution, deformation, and strains were presented and analyzed. In the second part, the measurements were compared with calculations using EBGEO (2010), and suggestions are given for improvements to this calculation model. In the test series, the vertical load parts on the piles, on the geosynthetic reinforcement (GR), and on the subsoil could be measured separately. This makes it possible to compare the test results with the separate parts of the analytical models. For the test conditions (static load, laboratory scale), smooth relationships were obtained between the net load on the fill (top load on fill minus subsoil support) and several measured parameters, such as load distribution and deformation. Consolidation of the subsoil resulted in an increasing load transferred through the GR, and also an increase of arching. The measured response to consolidation depends on the fill's friction angle. A higher friction angle gives more arching during consolidation. Loading on the geosynthetic reinforcement is concentrated on the strips lying above and between adjacent piles (the “GR strips”).

Two-part study concerned a series of twelve 3D laboratory model tests on piled embankments by van Eekelen *et al.* (2012b). In this second part, the measurements were compared with calculations made using the EBGEO (2010), CUR 226 (2010) analytical model, hereafter called ‘EBGEO’. Possible improvements to the analytical model are also suggested, and the resultant calculations are compared with the measurement results. EBGEO calculations consist of two steps: (step 1) load distribution in the fill i.e., arching behaviour, and (step 2) the load deflection behaviour of the geosynthetic reinforcement (GR). For the test conditions (static load, laboratory scale), it was found that the GR strains calculated using EBGEO are larger than the measured GR strains (approximately a factor of two for GR strains larger than 1%). The EBGEO calculations are

therefore too conservative. The following reasons were found. In step 1, the response of arching to subsoil consolidation in the experiments is different from that assumed in EBGEO. In step 2, the distribution of loading on the 'GR strips' lying between adjacent piles is quite different from that assumed by EBGEO, and EBGEO only takes part of the subsoil support into account. Modifications are suggested for the second calculation step. It is shown that this modified step 2 model results in significantly closer agreement with the test measurements.

Zhuang *et al.* (2014) presented a simplified model for analysis of an embankment of granular fill on soft ground supported by reinforcement and piles. This model was based on consideration of the arching effect in granular material proposed by Hewlett & Randolph. The vertical equilibrium of the unit body at the center of pile caps immediately below the reinforcement is established. The refinements of the model were that the failure mechanisms of the arch both at the crown and at the pile cap were considered, three-dimensional situation was taken into account for reinforced piled embankment, calculation of the vertical stress carried by the subsoil due to arching effect and reinforcement for multi-layered soil was proposed. Using the simplified model, the influence of embankment height, one-dimensional compression modulus of subsoil, tensile stiffness of reinforcement on stress reduction ratio (SRR) and tensile force of reinforcement was investigated. It was found that the model can be used to assess the relative contribution of the reinforcement and subsoil. The results showed that subsoil gives a major contribution to overall vertical equilibrium, while the reinforcement gives obvious contribution at relatively large settlement.

2. Arching concept

Arching is a phenomenon whereby the load is transferred laterally to stiffer elements. The soil between the piles is going to subside, however the soil above the piles cannot settle and will give resistance to the soil body that is subsiding. This causes shear forces and creates an arch (Van Eekelen and Bezuijen 2008). Its effect is widely observed, for instance in piled embankments, however, although this effect has been acknowledged for many decades, it remains quite poorly understood. There are several different empirical approaches which have been proposed to model the soil arching, but there does not yet exist a single method that can be agreed by the international geotechnical community.

3. Arching analysis

The concept of 'arching' of granular soil over an area where there is partial loss of support from an underlying stratum has long been recognized in the study of soil mechanics (Terzaghi 1943). Its effect is widely observed, for instance in piled embankments. However, although this effect has been investigated for many decades, it remains quite poorly understood. There are a number of different models from different theoretical mechanisms for piled embankment, but these models were not considered for embankments resting on stone columns.

A novel approach for determining the vertical loading on underground structures in granular soils has been developed by Iglesia *et al.* (1999) through combining experimental data from centrifuge 'trapdoor' tests with some theories on load redistribution due to arching. This approach creates the ground reaction curve (GRC), which is a plot of load on an underground structure as

the structure deforms causing the soil above it to arch

$$P^* = \frac{P}{P_0} \quad (1)$$

$$\delta^* = \frac{\delta}{B} \quad (2)$$

where:

P = the support pressure from the roof of the underground structure to the soil above (kN/m^2),
 P_0 = the nominal overburden total stress at the elevation of the roof derived from the thickness of overlying soil (and any surcharge at the ground surface) (kN/m^2),
 B = the width of the underground structure (m), and
 δ = the settlement of the roof (m).

4. Initial arching

The GRC starts with the geostatic condition ($P_0 = \gamma h$). The initial ‘convergence’ of the soil toward the underground structure causes a fairly abrupt reduction in load on the structure. In this phase, the arch starts to form. A modulus of arching (MA) is defined as the rate of initial stress decrease in the normalized plot. Iglesia *et al.* (1999) proposed that based on the centrifuge trapdoor experiments with granular media, the modulus of arching has a value of about 125. Thus p^* tends to zero (or its minimum value) when $\delta^* > 1\%$.

5. Break point and relative arching ratio

As the underground opening converges toward a state of maximum arching (minimum loading), the GRC changes from the initial linear line to a curve (since p^* can only approach zero and certainly cannot be negative).

6. Maximum arching

Maximum arching occurs when the vertical loading on the underground structure reaches a minimum. Iglesia *et al.* (1999) described this corresponding to a condition in which a physical arch forms a parabolic shape just above the underground structure. In addition, this tends to occur when the relative displacement between the underground structure and the surrounding soil is about 2 to 6 % of the effective width of the structure (B).

7. Loading recovery stage

This stage is the transition from the maximum arching (minimum loading) condition to the ultimate state (where the arch has become a prism with vertical stress sides as proposed by

Terzaghi (1943). Iglesia *et al.* (1999) characterized this stage by the load recovery index (λ). Based on centrifuge tests, it was shown that the load recovery index increases with increasing B/D_{50} (D_{50} is the average particle size) and decreasing h/B (where h is the overburden depth). This aspect of behavior is potentially of considerable significance, since it represents ‘brittle’ arching response. As the surrounding soil continually converges toward the underground structure, the arch will eventually collapse.

A trial was made by Fattah and Majeed (2012) to improve the behaviour of stone column by encasing the stone column with geogrid as reinforcement material. The program CRISP-2D was used in the analysis of problems. The program allows prediction to be made of soil deformations considering Mohr-Coulomb failure criterion for elastic–plastic soil behavior. A parametric study was carried out to investigate the behavior of standard and encased floating stone columns in different conditions. Different parameters were studied to show their effect on the bearing improvement and settlement reduction of the stone column. These include the length to diameter ratio (L/d), shear strength of the surrounding soil and, the area replacement ratio (a_s) and others. It was found that the maximum effective length to diameter (L/d) ratio is between (7-8) for C_u , between (20-40) kPa and between (10-11) for $C_u=10$ kPa for ordinary floating stone columns while the effective (L/d) ratio is between (7-8) for encased floating stone columns. The increase in the area replacement ratio increases the bearing improvement ratio for encased floating stone columns especially when the area replacement ratio is greater than (0.25). The geogrid encasement of stone column greatly decreases the lateral displacement compared with ordinary stone column.

In this paper, the embankment model is supported by stone columns instead of piles. The analyses focus on arching in the embankment models over ordinary and encased stone columns and the effect of the subsoil is represented by a uniform vertical stress of soil. Different factors such as spacing between columns, length to diameter ratio and embankment height are included in the analysis.

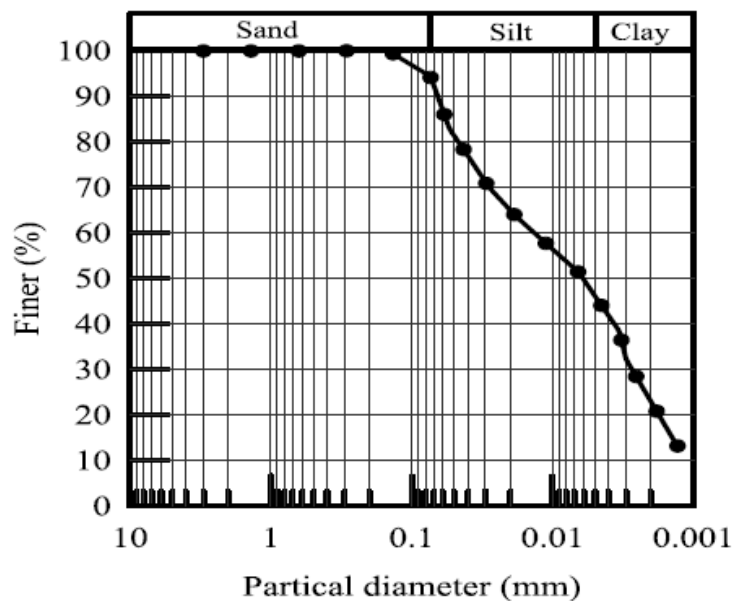


Fig. 1 Grain size distribution of clayey soil used

Table 1 Physical and chemical properties of natural soil used

Property	Value
Liquid limit (LL) %	47
Plastic limit (PL) %	23
Plasticity index (PI) %	24
Specific gravity (G_s)	2.7
% Passing sieve No. 200	94
Sand content % (0.075 to 4.75 mm)	6
Silt content % (0.005 to 0.075 mm)	48
Clay content % (< 0.005 mm)	46
Maximum dry unit weight (kN/m^3)	18.24
Optimum moisture content (%)	13
Total soluble salts (%)	6.13
SO ₃ (%)	0.6
Organic matter (%)	1.09
Gypsum content (%)	1.17
pH	8.34

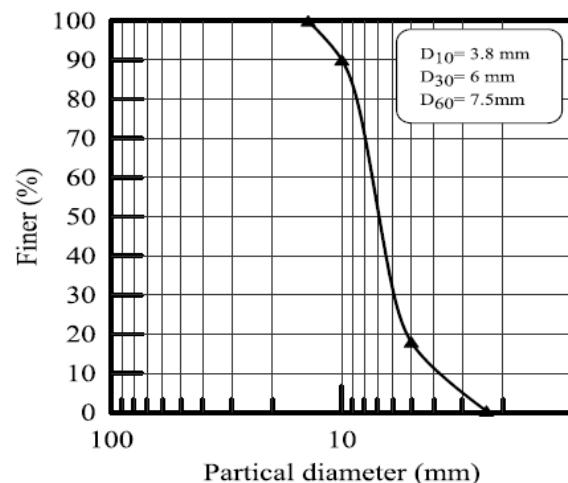


Fig. 2 Grain size distribution of the stone used

8. Experimental work

A brown lean clay soil was brought from a depth of 5 m in a site within Al-Basrah government south of Iraq. The soil was subjected to routine laboratory tests to determine its properties, these tests included: grain size distribution (sieve analysis and hydrometer tests) according ASTM D422 specifications, Atterberg limits (liquid and plastic limits) according to ASTM D4318 and specific gravity according to D854 specifications. The results revealed that the soil consists of 6% sand, 46% clay and 48% silt as shown in Fig. 1. The soil is classified according to the Unified soil classification system USCS as (CL). Table 1 shows the physical and chemical properties of the soil used.

Table 2 Physical properties of the crushed stone

Property	Value
Maximum dry unit weight (kN/m^3)	15.7
Minimum dry unit weight (kN/m^3)	13
Dry unit weight (kN/m^3) at	
$D_r=55\%$	14.4
D_{10} (mm)	3.8
D_{30} (mm)	6
D_{60} (mm)	7.5
Coefficient of uniformity (C_u)	1.97
Coefficient of curvature (C_c)	1.26
Angle of internal friction (θ°)	41.5
Specific gravity (G_s)	2.65

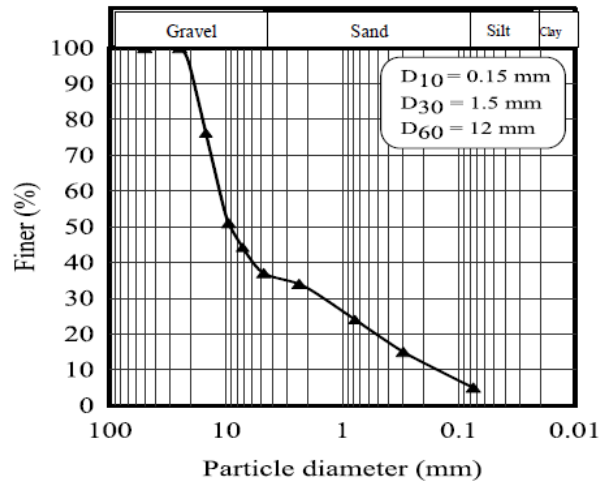


Fig. 3 Grain size distribution of the sub-base used

9. Crushed stone

The crushed stone, used as a backfill material was obtained from a private gravel factory. The size of the crushed stone was chosen in accordance with the guidelines suggested by Al-Shaikhly (2000), where the particle size is about 1/7 to 1/9 of the diameter of stone columns. The particle size distribution is shown in Fig. 2, the particle sizes range between 2 to 14 mm and found to have an angle of internal friction of 41.5° from direct shear test at a dry unit weight of 14.4 kN/m^3 corresponding to a relative density of 55%. The stone is uniform as its uniformity coefficient is less than 4 and considered as poorly graded. The physical properties are presented in Table 2.

10. Embankment fill material

The granular sub-base was brought from Al-Nibae quarry, north of Baghdad. The sub-base is

Table 3 Physical and chemical properties of the sub-base (fill) material used

Property	Value
CBR (%)	51
Maximum dry unit weight (kN/m ³)	21.84
Optimum moisture content (%)	6.3
D_{10} (mm)	0.15
D_{30} (mm)	1.5
D_{60} (mm)	12
Coefficient of uniformity (C_u)	80
Coefficient of curvature (C_c)	1.25
Angle of internal friction (ϕ^o)	40
SO ₃ (%)	0.23
Total soluble salts (%)	2.93
Gypsum content (%)	0.494
Organic matter (%)	0.057

Table 4 Physical and mechanical properties of the geogrid used

The physical properties	Data	
Mesh type	Square	
Color	Green and Blue	
Polymer type	HDPE	
Packaging	Rolls	
Dimensional Properties	Unit	Data
Aperture size	mm	10 × 10
Mass per unit area	g/m ²	318
Rib thickness	mm	1.7
Junction thickness	mm	1.6
Roll width	m	1.2
Roll length	m	30
Mechanical Properties	Unit	Data
Peak tensile resistance	kN/m	0.62
Elastic modulus	MPa	40
Tensile strength	MPa	0.44
Percentage elongation at maximum load	%	1.4
Yield strength at 10% strain	kN/m	0.47

commonly used as a fill material for embankment construction. Fig. 3 shows the grain size distribution of sub-base material according to (B.S.1377 1990, Test 7B). The physical and chemical properties of the sub-base used are shown in Table 3. The sub-base is classified as (GW) according to USCS.

11. Geogrid reinforcement

The geogrid material used for this study is Pars Mesh Polymer (PMP) Type SQ12 manufactured by the Iranian company Pars Mesh Polymer. Tension tests were performed on geogrid as per ASTM D6637 to determine its strength and tensile modulus. From the load-strain data, the tensile modulus, M (secant slope of stress-strain curve) was 79 kN/m and its yield strength was taken as 0.47 kN/m at 10% strain level. Table 4 summarizes the physical and mechanical properties of geogrid used.

12. Model design and manufacturing

To study the behavior of soft clay reinforced by ordinary and geogrid encased stone columns underneath embankment; an experimental setup with an approximate scale of 1/20 to 1/30 of the prototype was designed and manufactured to achieve this goal. The setup consists of: steel container, loading frame, hydraulic system, load cell with load indicator, earth pressure cell, piezometer, strain gauge with strain indicator, footing model, dial gauges and data acquisition.

13. The test setup

Steel container: A movable steel container was constructed to host the bed of soil and all accessories. The internal dimensions are 1500 mm length, 800 mm width and 1000 mm depth. The container was made of steel plates 6 mm in thickness braced externally by angles at their corners, edges and each side. The front side was made from tough glass. The container was provided with four wheels that allow it to move freely, the container is sufficiently rigid and exhibited no lateral deformation during preparation of soil and during the test. Fig. 4 shows details of the container.



Fig. 4 Experimental test container and loading system



Fig. 5 Earth pressure cell model 4800

Loading frame and axial loading system: The steel frame consists of two columns and a beam, each column is fixed at bottom by casting in a concrete slab. The axial pressure is applied through a hydraulic system which consists of three hydraulic jacks; one in the middle and the others on sides, used to apply the load on the embankment model, the location of the hydraulic jack is shown in Fig. 4. The maximum stress that can be applied on a model footing (250 mm×500 mm) reaches about 400 kPa. The pressure is measured by a load cell 50 kN in capacity connected to the digital load indicator.

Earth pressure cell and readout: Earth pressure cells provide a direct means of measuring total pressure in or on bridge abutments, diaphragm walls, fills and embankments, retaining walls surfaces, sheet piling, slurry walls and tunnel lining. They may also be used to measure earth bearing pressure on foundation slabs and footings and at the tips of piles. Fig. 5 shows the earth pressure cell model 4800 manufactured by GEOKON company in U.S.A which is used in this study. Earth pressure cells are constructed from two thin stainless steel plates welded together around their periphery and separated by a narrow gap filled with hydraulic fluid. A length of stainless steel tubing connects the fluid filled cavity to a pressure transducer that converts the fluid pressure into an electrical signal transmitted by cable to the readout. They can be positioned in the fill at different orientations so that soil pressure can be measured in two or three directions.

Strain gauge and strain readout: Strain can be used for measurement of acceleration, velocity and displacement. It can be applied for measuring of vibrations in a wide frequency range. Plug-in amplifiers; Multi-channels designed (16 channels) of 120 ohm. The readout is connected to computer for output data, it converts the electric (DC) wave to readings in (μ s) measured with time under each load.

14. Preparation of model tests

Prior to the preparation of the soil bed in the container, the variation of shear strength of the clayey soil with time after mixing at different liquidity indices should be obtained. Therefore; six samples with different liquidity indices were prepared individually; each sample was placed in five

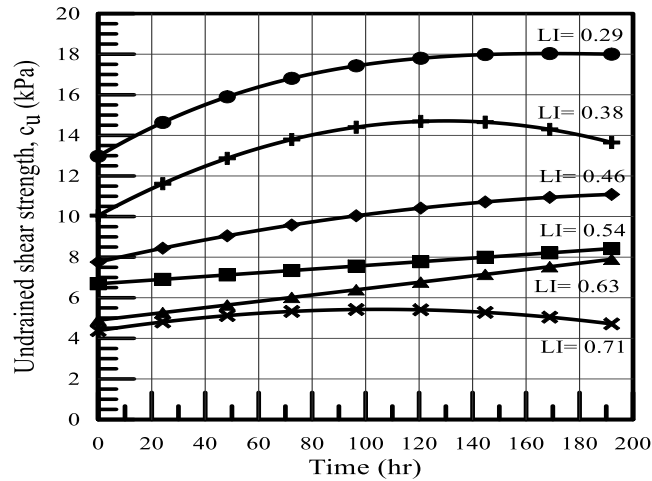


Fig. 6 Variation of the undrained shear strength with liquidity index

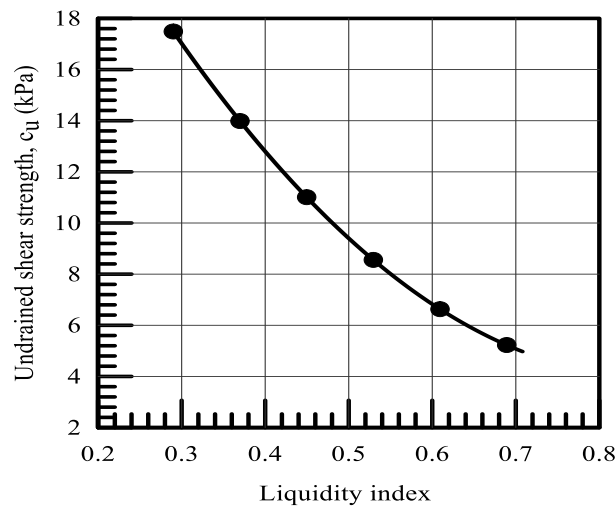


Fig. 7 Variation of undrained shear strength with time after mixing

layers inside a CBR mold. Each layer was tamped gently with a special hammer to extract any entrapped air. The samples were then covered with polyethylene sheet and left for a period of eight days. Each day, the undrained shear strength was measured by a portable vane shear device. These tests provide the time required for the remolded soil to regain strength after a rest period following the mixing process, Fig. 6. The shear strength of soil decreases with the value of liquidity index and the influence of time decreases with liquidity index, Fig. 7 shows the variation of shear strength of soil with liquidity indices after 96 hour curing.

According to the results obtained from Fig. 7, the soil was prepared in the manufactured container at undrained shear strength c_u of 10 kPa and liquidity index of 0.48 corresponding to water content of 34.5%. To perform soil preparation, 660 kg of air dried soil was divided into 30 kg groups; each group was mixed separately with enough quantity of water to get the desired consistency. The mixing operation was conducted using a large mixer manufactured for this



Fig. 8 Strain gauge fixed on geogrid



Fig. 9 Process of construction of encased stone columns

purpose till completing the whole quantity. After thorough mixing, the wet soil was kept inside tightened polythen bags for a period of one day to get uniform moisture content. After that, the soil was placed in a steel container (1500×800×1000) mm in eleven layers; each layer was leveled gently using a wooden tamper of dimensions (50×100) mm. This process continues for the eleven layers till reaching a thickness of 560 mm of soil in the steel container. After completing the final layer, the top surface was scraped and leveled to get, as near as possible, a flat surface, then covered with polythen sheet to prevent any loss of moisture as shown in Plate 8. A wooden board of area similar to that of the soil surface area (1500× 800) mm was placed on the soil bed. The prepared soil was left for a period of four days to regain its strength reaching 10 kPa as was suggested by Fattah *et al.* (2011).

14.1 Installation of the stone columns

The position of the stone columns to be placed correctly in their proper locations was marked using a special frame manufactured according to the proposed configuration patterns of stone columns. A hollow steel pipe with external diameter of 70 mm coated with petroleum jelly was pushed down the bed to the specific depth (560 mm in fully penetrated stone column with $L/d=8$

and 350 mm for partially penetrated stone column with $L/d=5$) with the aid of the loading system. To remove the soil inside the casing, a hand auger, manufactured for this purpose was used. After that, the casing was removed carefully. The stones were carefully charged into the hole in ten layers and compacted at relative density of 55% using 50 mm diameter rod to achieve a dry unit weight of 14.4 kN/m^3 by a tamping rod.

14.2 Installation of encased stone columns

To install the encased stone columns, the same procedure of the construction of ordinary stone columns was followed. First, formed samples of geogrid tubes were made by warping up a roll of geogrid and sewing by a nylon and strings with a diameter of 68 mm and length of the encased stone column for $L/d=8$ and $L/d=5$. Then strain gauges were fixed on the tube of geogrid in predetermined positions using glue and covered by flexible putty as shown in Fig. 8. A hollow steel pipe with external diameter of 70 mm was pushed down to the soil bed to the specific depth; then a hand auger is used to remove the soil inside the steel pipe. Then, a geogrid tube was inserted into the stone column hole using the steel pipe as shown in Fig. 9.

14.3 Installation of embankment fill

The construction of the embankment fill was started after installation of ordinary stone columns. A predetermined weight of sub-base was mixed with water by a mixer at optimum moisture content of 6.3%, this weight of sub-base is sufficient to create a uniform layer 50 mm thick. Each layer was compacted gently by a wooden tamper of size $75 \times 75 \text{ mm}$ to attain a placement maximum dry unit weight of 21.84 kN/m^3 until the desired embankment depth is obtained. Then the top layer was leveled using a piece of plywood. The final upper width of the embankment is 300 mm. Fig. 10 shows the process of preparation of the embankment.

15. Model testing procedure

The model tests were carried out on natural soil and soil improved with ordinary stone columns. The load cell and load readout used in testing program were calibrated by applying



Fig. 10 Installation of embankment fill

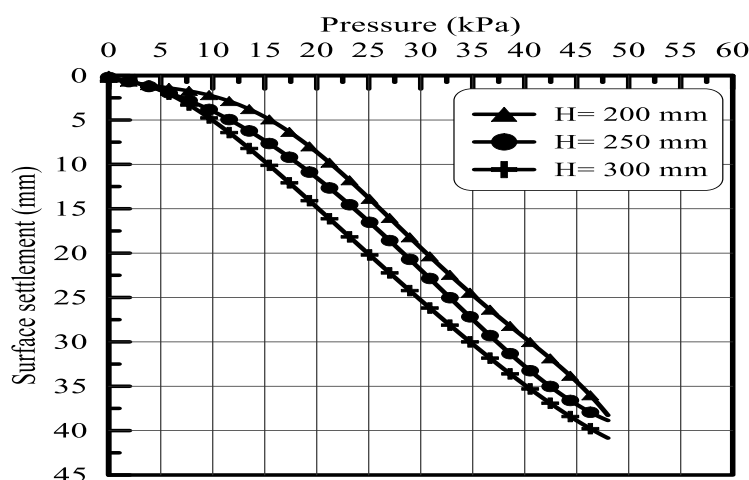


Fig. 11 Bearing ratio versus settlement ratio for untreated embankment model

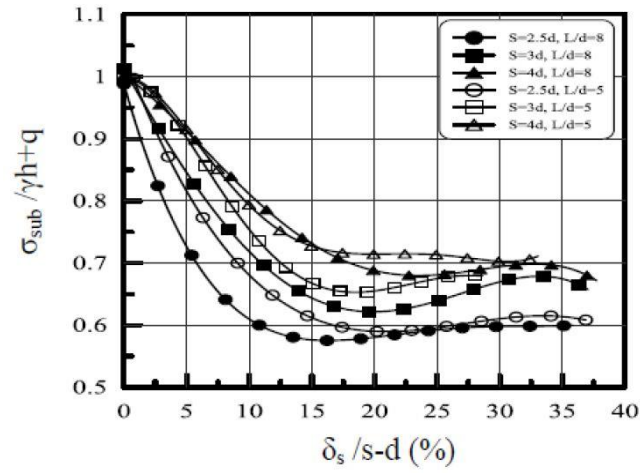
different known static loads and measuring values through the load cell before using. A footing (250 mm×600 mm) in dimensions was placed in position on the surface of the embankment model so that the center of the footing coincides with the center of the load cell and hydraulic jack. Loads were then applied through a hydraulic jack in the form of load increments and measured by the load cell and recorded by load readout. During each load increment, the readings of the three dial gauges were recorded. The dial gauge readings were recorded at the end of the period of each load increment. Each load increment was left for 5 minutes; the load increment was applied till the rate of settlement became constant.

16. Presentation and discussion of test results

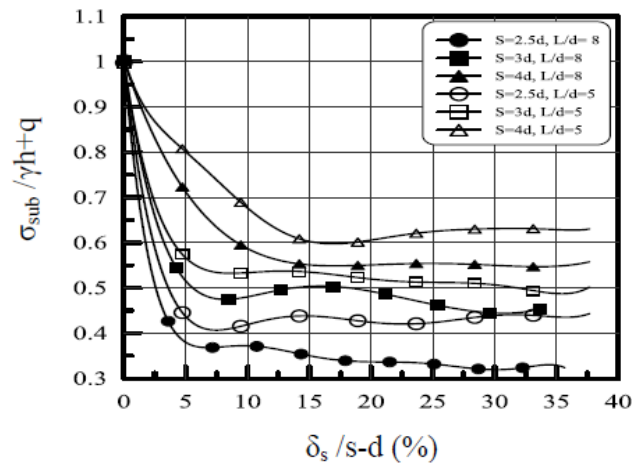
The investigation focuses on influence of parameters like, spacing of stone columns, length of stone column and height of embankment on overall behavior of soft soil treated by ordinary stone columns (OSC). The analysis of results of all model tests regarding the applied stress and the corresponding settlement is illustrated in terms of (q/c_u) vs (S/B) . The (q/c_u) represents the ratio of applied stress to undrained shear strength of the soft clay, denoted as “bearing ratio” and (S/B) represents the corresponding vertical settlement as a percent of the model footing width, denoted as “settlement ratio”. To obtain the degree of improvement achieved by each improvement technique, the results are plotted in the form of $(q/c_u)_t / (q/c_u)_{unt}$ denoted as “bearing improvement ratio”, where $(q/c_u)_t$ is improved bearing ratio and $(q/c_u)_{unt}$ is unimproved bearing ratio. The improvement in settlement achieved by the model tests is presented in the form of (S_t/S_{unt}) “settlement of treated soil to settlement of untreated soil at the same applied stress” denoted as “settlement improvement ratio”, plotted against the bearing ratio (q/c_u) .

The failure point is defined when the settlement reaches 36% of the diameter of the stone column or 10% of the width of the model footing. This definition is compatible with Terzaghi (1943).

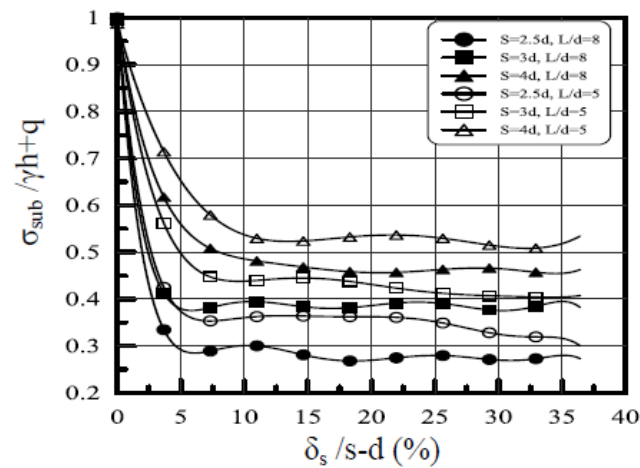
Fig. 11 shows the bearing ratio plotted against settlement ratio, the figure illustrates that the mode of failure of model test is close to local shear pattern, due to the rapid rate of deformation. In



(a) $h=200$ mm



(b) $h=250$ mm



(c) $h=300$ mm

Fig. 12 Normalized ultimate soil stress with normalized settlement for different spacing ratios

this test, the footing model is resting on compacted layer (sub-base) of width relatively \approx the footing width. The ultimate bearing capacity obtained is 35 kPa, 33 kPa and 30 kPa for the model tests of embankment height 200 mm, 250 mm and 300 mm respectively based on the failure criterion of 10% of footing width. The figure demonstrates that the soil bed underneath the 200 mm embankment height exhibited higher bearing ratio. The bearing ratios at failure (q/c_u) for the embankment- soft soil model are 3.5, 3.3 and 3.0 corresponding to the settlement ratio of 10% of the footing width and for embankment heights 200, 250 and 300 mm respectively. The results demonstrate a substantial decrease in bearing ratio with increasing thickness of embankment; this is due to the increase in the settlement induced by the load from embankment and applied stress.

17. Embankment models over soft soil treated by ordinary stone columns

17.1 Stress on subsoil

The subsoil stress (σ_{sub}) is normalized by the nominal overburden stress at the base of the embankment ($\gamma h + q$), initially is one before there is a tendency for arching (before loading, $\delta s = 0$), corresponding settlement at the surface of the embankment will now be referred to as δs . This settlement is normalized by the clear spacing between the stone columns ($s-d$), which is equivalent to the width of the structure. Fig. 12 shows normalized subsoil stress (σ_{sub}) with normalized settlement for different spacing ratios; length to diameter ratios and embankment heights.

The results show that the normalized soil stress increased as the spacing between columns increased and length to diameter ratio decreased for the given height of embankment. This is due to reduced stress concentration on columns by soil arching and more punching of stone columns. In addition, the point of maximum arching (minimum soil stress) is reached at a displacement about 2 % to 7 % for embankment models of 250 mm and 300 mm height while the models of 200 mm height reach minimum soil stress at large displacement as the spacing ratio increased and length to diameter ratio decreased. This behavior may be attributed to the increase in displacement of soil between stone columns due to increase of redistribution of load from the embankment to the subsoil and dispersed soil arching effect as the embankment height decreased.

17.2 Soil arching ratio (ρ) or stress reduction ratio (SRR)

The ratio ($\sigma_{sub} / \gamma h + q$) is defined as the soil arching ratio or stress reduction ratio (SRR) which represents the minimum stress on the subsoil (σ_{sub}) at the point of maximum arching. This ratio variation with embankment height (h) is shown in Fig. 13 which shows that for $h > 250$ mm, soil arching ratio reduces slowly and becomes approximately constant as embankment height increased for L/d ratio = 5 and 8, but when $h < 250$ mm, soil arching ratio increases rapidly, tending towards 1.0 that represent all the external stress carried by the soil. In addition, it can be observed from this figure that as the spacing ratio increased, the arching ratio increased, this means that the much load of embankment is carried by the subsoil between stone columns. The figure also reveals that reduced L/d ratio leads to increase soil arching ratio.

Fig. 14 shows the variations of soil arching ratio or (SRR) with h normalized by ($s-d$). It can be noticed that for $h > 1.2 (s-d)$, soil arching ratio reduces slowly as h increases, but when $h < 1.2 (s-d)$, soil arching ratio increases rapidly, tending towards 1.0. Also as previously noted, the value of soil arching ratio tends to increase with (s).

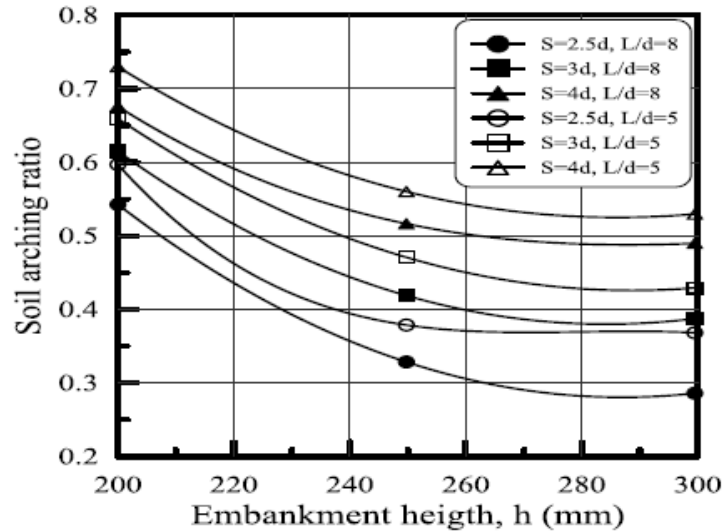


Fig. 13 Soil arching ratio variation with embankment height (h) for different spacing ratios and L/d ratios

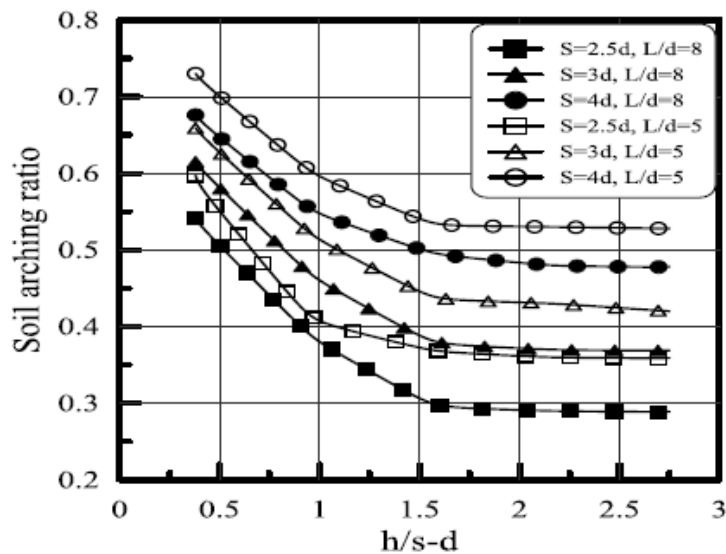


Fig. 14 Soil arching ratio variation with embankment height (h) normalized by $(s-d)$ for different spacings and L/d ratios

It can be observed from this figure that there is virtually no effect of arching when $h < 1.2 (s-d)$, because the stress acting on the subsoil is large and the settlement at the surface of the embankment is too much.

For $1.2 (s-d) \leq h \leq 2.2 (s-d)$, there is increasing evidence of arching; as (h) increases, the settlement at the surface of the embankment reduces, and the stress acting on the subsoil reduces compared to the nominal overburden stress.

For $h > 2.2 (s-d)$, “full” arching is observed; there is small settlement at the surface of the

embankment, and the stress acting on the subsoil is considerably reduced compared to the nominal overburden stress.

Critical heights from experimental data for the present study based on soil arching formed will be

$$HC = 1.2 (s-d) \text{ to } 2.2 (s-d) \quad (3)$$

This figure illustrates that the embankment height and spacing ratio play a considerable part in the design of piled (stone column) embankment system.

18. Stress concentration ratio

The ratio of the vertical stress in the stone column to the vertical stress in the surrounding soft soil is defined as the stress concentration ratio. In this study, these stresses were measured directly and the change in pore water pressure was accounted, therefore, the stress concentration ratio was measured in terms of effective stresses.

Fig. 15 shows the variation of stress concentration with embankment height for different spacing ratios and L/d ratios. It is observed that, for different magnitudes of embankment height, stress concentration ratio increases and reaches a maximum value, then maintains nearly a constant value. The higher value of embankment height at ($L/d=8$), the higher the stress concentration ratio, due to soil arching effect. A higher value of stress concentration ratio indicates that a higher percentage of the embankment load is transferred to stone columns. These results revealed that the stress concentration ratio is influenced by the embankment height and spacing ratio between columns. These results are in good agreement with the experimental results of piled embankment models by Chen *et al.* (2008), Britton and Naughton (2008) who studied the effect of embankment height, pile cap to clear spacing ratio and reinforcement tensile strength on the arching.

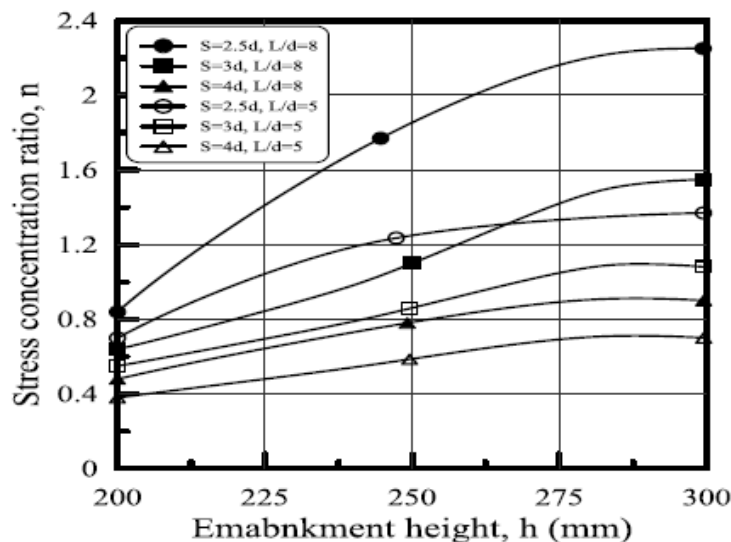


Fig. 15 Stress concentration ratio at failure versus embankment height for different spacing ratios and L/d ratios

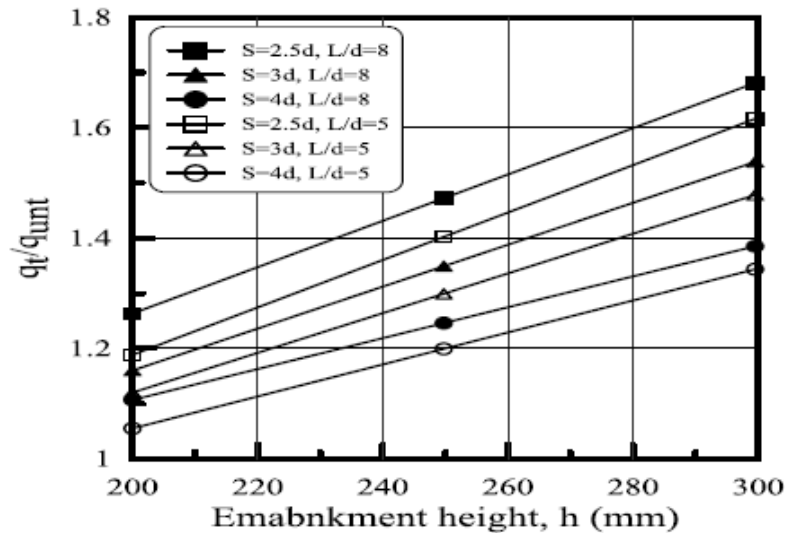


Fig. 16 Bearing improvement ratio at failure versus embankment height for models treated by ordinary stone columns

19. Bearing improvement ratio versus embankment height

Fig. 16 shows variation of the bearing improvement ratio for embankment models resting on soft ground strengthened by ordinary stone columns with (h). The relation is almost linear for all column spacings and L/d ratio, from this figure, it can be observed that as the embankment height increases, the bearing improvement ratio increases due to stress concentration on column and reduced stress on subsoil. This is because the soil arching effect leads to decrease settlement between stone columns due to transfer of the embankment load and external pressure to the stone columns and the higher value of bearing improvement ratio indicates that a higher percentage of the embankment load is transferred to stone column at the same spacing ratio for both $L/d=5$ and 8. In addition, it can be noticed from the figure that as the spacing between columns increases, the effect of soil arching decreases and little values of bearing improvement ratio are obtained.

20. Settlement improvement ratio

Variation of settlement improvement ratio S_t/S_{unt} versus embankment height (h) for different column spacings is shown in Fig. 17. This relation is also linear, the results imply that as (h) increases, the soil arching effect is sufficient too much and the amount of embankment load will be carried by the stone columns and the amount of displacement required for achieving ultimate arching conditions decreases that will be reflected to the top of the embankment, also the amount of stress redistribution from the subsoil to the stone column increases. This observation is also consistent with variation of spacing, which indicates more settlement as spacing increases for a given h and L/d ratio=5 and 8. These results are in good agreement with Jenck *et al.* (2006), Britton and Naughton (2008) results from experimental tests. They conducted that settlement is significantly affected by the height of the embankment and the pile cap spacing ratio.

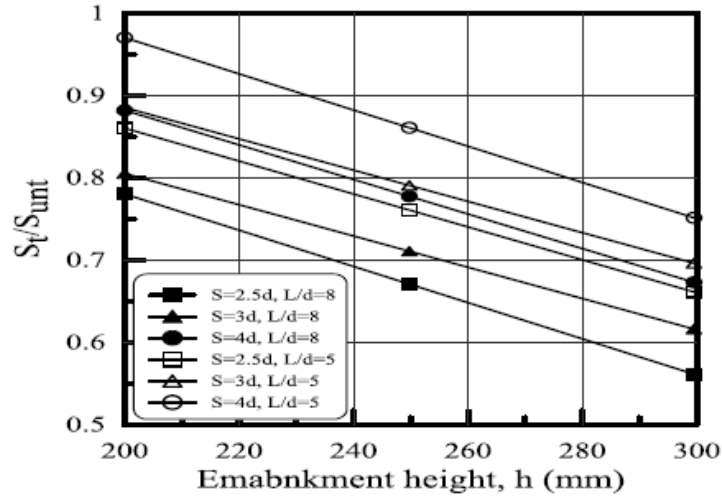


Fig. 17 Settlement improvement ratio at failure versus embankment height for models treated by ordinary stone columns

21. Embankment models resting on soft soil treated by encased stone columns

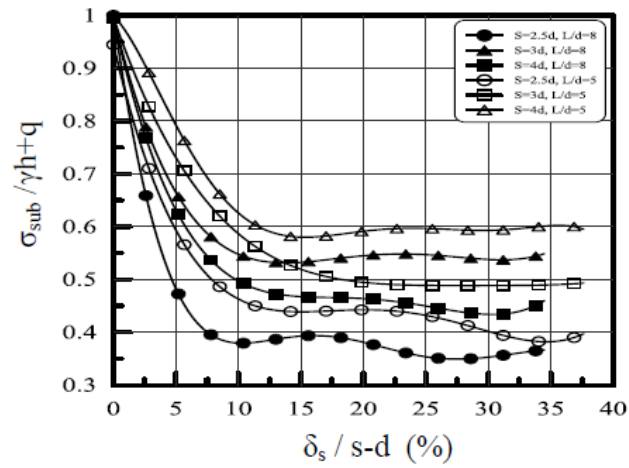
21.1 Stress on subsoil

Fig. 18 shows normalized subsoil stress (σ_{sub}) with normalized settlement for different spacing ratios; length to diameter ratios and embankment heights for embankment models on encased stone columns.

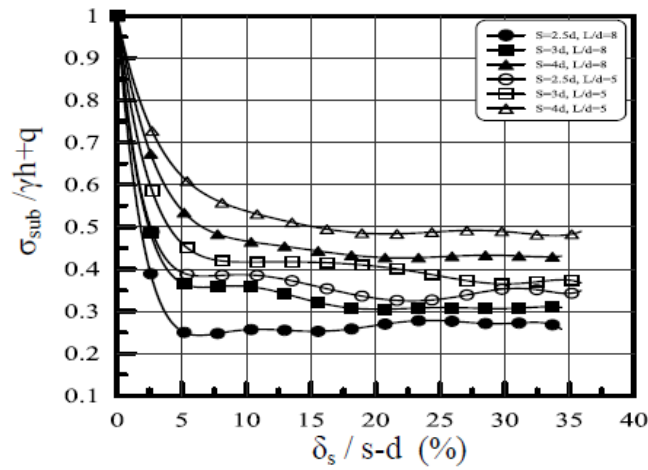
The results show that the normalized soil stress increases as the spacing between columns increases and length to diameter ratio decreases for the given height of embankment. The use of encasement for both end bearing and floating columns leads to reducing the ultimate stress on the subsoil to about 30% to 50% of that stress in the model of ordinary stone columns. This may be attributed to the fact that encasement increases the stress concentration on stone columns by increasing the stiffness of column and from the effect of soil arching, small present of stress will be carried by the subsoil. In addition, the figure illustrates that a little settlement in the embankment surface occurs with a minimum stress on subsoil as the height of embankment increases.

21.2 Soil arching ratio (ρ) or stress reduction ratio (SRR)

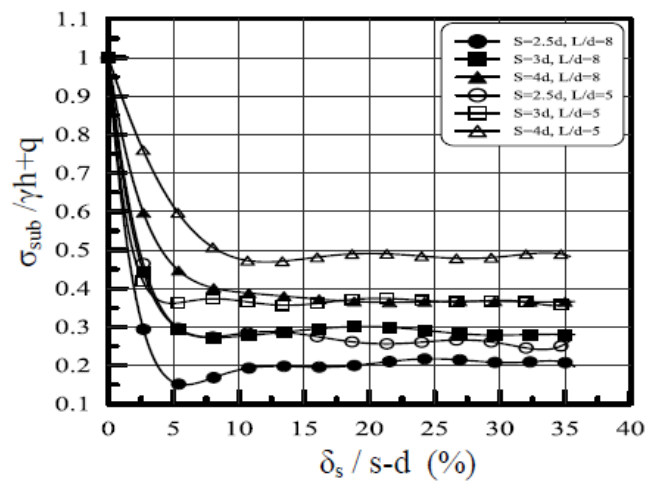
Figs. 19 and 20 show the effect of embankment height on the soil arching ratio (minimum stress on subsoil) for OSC and ESC models with L/d ratio=5 and 8 respectively. It is noticed from figures that for $h > 250$ mm, soil arching ratio reduces slowly and becomes approximately constant as the embankment height increased but when $h < 250$ mm, the soil arching ratio increases rapidly, tending towards 1.0. This finding is in agreement with numerical results of pile embankment by Han and Gabr (2002). In addition, it can be observed from these figures that as the spacing ratio increases, the arching ratio increases, and slight difference in value was found between model treated with ESC at $s=3d$ and $s=4d$ and model treated with OSC at $s=2.5d$ and $s=3d$ for $h \geq 250$ mm. This indicates, through soil arching action, that the external and embankment loads are transferred



(a) $h=200$ mm



(b) $h=250$ mm



(c) $h=300$ mm

Fig. 18 Normalized ultimate soil stress with normalized settlement for different spacing ratios

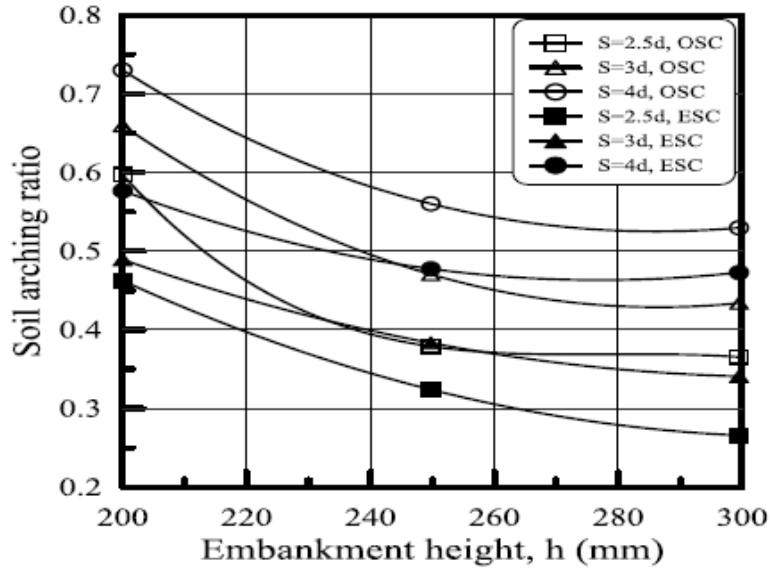


Fig. 19 Soil arching ratio variation with embankment height (h) for different spacing ratios and L/d ratio=5

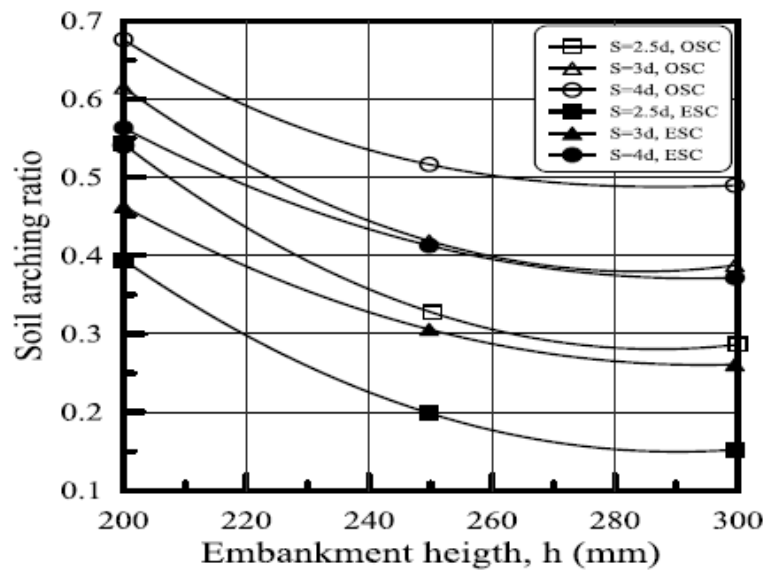


Fig. 20 Soil arching ratio variation with embankment height (h) for different spacing ratios and L/d ratio=8

to the stone columns, so for stone column embankment system with reinforcement, a larger spacing ratio can be used. Also reducing L/d ratio leads to increase the soil arching ratio due to increase of the stress on the subsoil with decreasing stress on stone columns. The lateral deformation of floating columns will reduce due to loss of end bearing and that causes increase of the settlement of the subsoil and vertical deformation of stone column through punching of OSC and ESC.

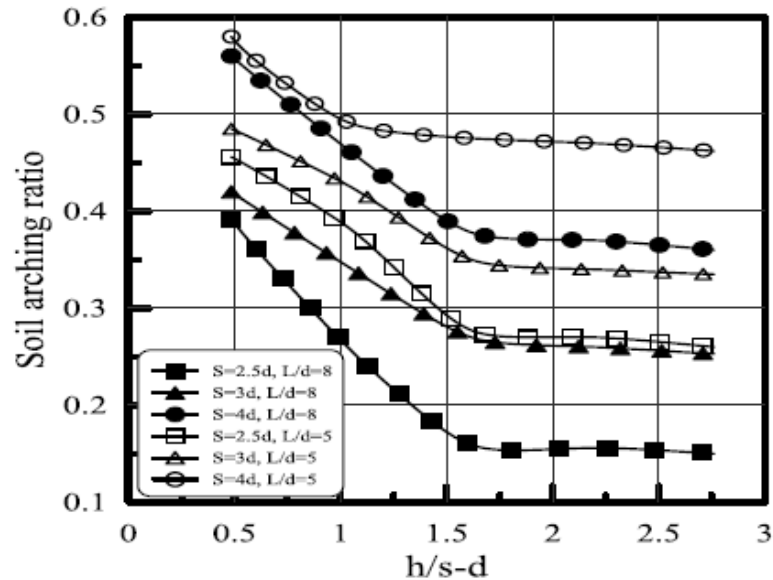


Fig. 21 Soil arching ratio variation with embankment height (h) normalized by ($s-d$) for different spacing ratios and L/d ratios

Fig. 21 shows the variations of soil arching ratio with (h) normalized by ($s-d$). When $h < 1.4 (s-d)$, no effect of arching can be observed from this figure, because the soil arching ratio ≈ 1.0 and stress acting on the subsoil is large with high settlement at the surface of the embankment for both L/d ratios.

For $1.4 (s-d) \leq (h) \leq 2.2 (s-d)$, there is increasing evidence of arching as (h) increases, the settlement at the surface of the embankment reduces, and the stress acting on the subsoil reduces compared to the nominal overburden stress.

For $h > 2.2(s-d)$, “full” arching is observed; there is small settlement at the surface of the embankment, and the stress acting on the subsoil is considerably reduced compared to the nominal overburden stress.

Critical height from experimental data for the present study of encased stone columns embankment system will be

$$HC = 1.4 (s-d) \text{ to } 2.2 (s-d) \quad (4)$$

It is observed that the critical height value increases when using encased stone columns under the embankment models with small spacing ratio.

Table 5 summarizes the range of critical height for different studies and theoretical analyses. The value of the present study is compared with these data from literature and a good agreement is obtained with the value suggested by Terzaghi (1943), Hewlett and Randolph (1988), Naughton (2007) who studied piled embankment models.

The comparison shown in Table 5 indicates that the behavior of stone column-embankment is similar to that of piled embankment and the stone columns play the same role of piles in stress distribution. The table gives rise to the stone – column embankment and can be used for selecting the design criteria based on spacing of stone columns underneath embankments.

Table 5 Summary of the range of critical heights for arching

Design method / experimental investigation	Critical height (H_c)
Terzaghi (1943)	2.5 ($s-d$)
BS8006 (1995)	1.4 ($s-d$)
Hewlett and Randolph (1988)	1.4 ($s-d$)
Kempfert (2004)	s/d
Naughton (2007)	1.25 ($s-d$) 2.4 ($s-d$)
Horgan and Sarsby (2002)	1.545 ($s-d$) 1.92 ($s-d$)
Ellis and Aslam (2008)	2.0 ($s-d$)
Russell <i>et al.</i> (2003)	H
Present study for embankment models on OSC.	1.2 ($s-d$) 2.2 ($s-d$)
Present study for embankment models on ESC.	1.4 ($s-d$) 2.2 ($s-d$)

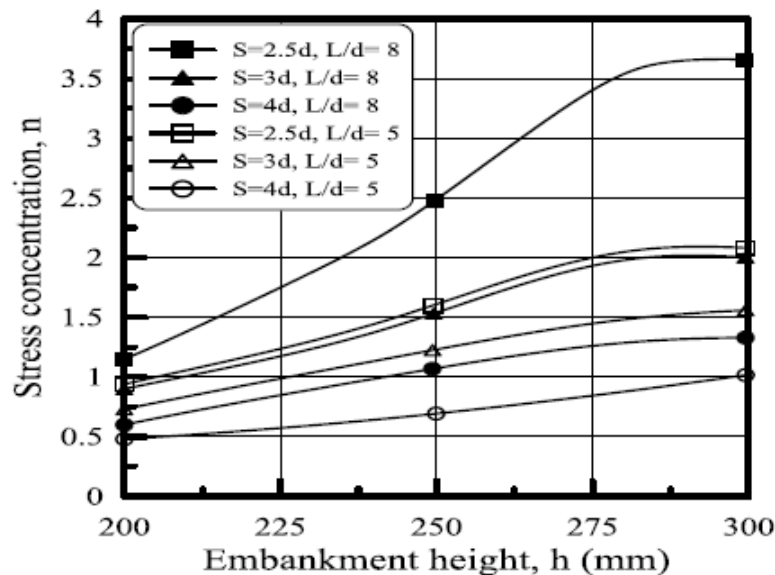


Fig. 22 Stress concentration ratio at failure versus embankment height for different spacing ratios and L/d ratios

21.3 Stress concentration ratio

Fig. 22 shows the variation of stress concentration ratio with embankment height for encased stone columns model. It is observed that, for different spacing ratios and L/d ratio=5 and 8, the stress concentration ratio increases with increasing (h). The higher value of embankment height and $L/d=8$ with encased stone columns, the higher the stress concentration ratio, this is due to soil arching effect. A higher value of stress concentration ratio indicates that a low percentage of the embankment load and external load is transferred to subsoil. In addition, the figure illustrates that using floating encased stone columns at spacing $s=2.5d$ gives concentration ratio closer to value of model treated by end bearing encased stone columns at spacing $s=3d$.

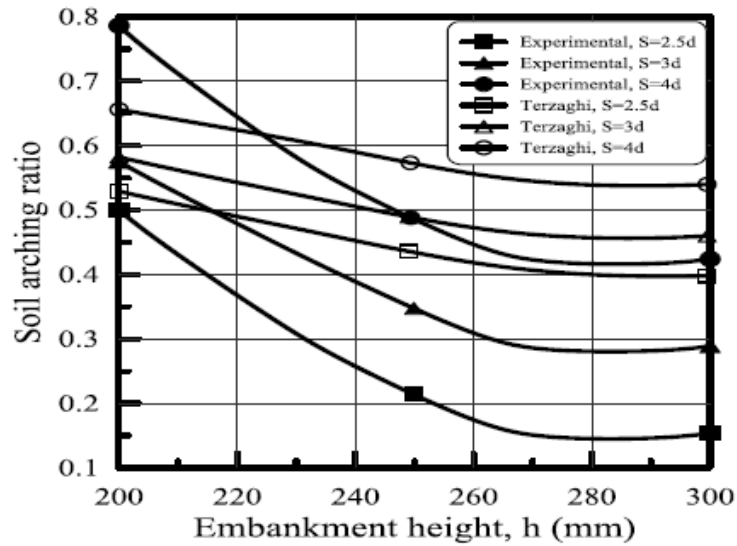


Fig. 23 Comparison between the test results and Terzaghi (1943) design method for soil arching ratio

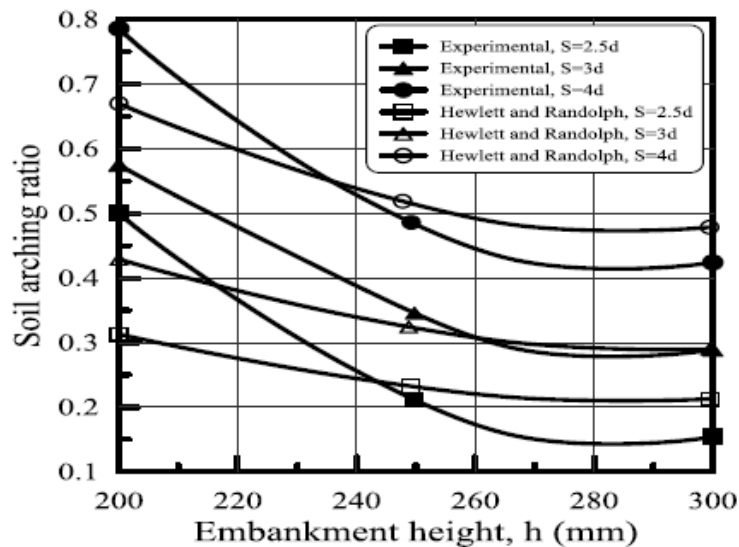


Fig. 24 Comparison between the test results and Hewlett and Randolph (1988) design method for soil arching ratio

22. Comparisons of theoretical design methods with experimental results

A number of research studies associated to describe soil arching but none of the design methods for soil arching stated in this section considers the influence of stone columns reinforcement, length to diameter ratio and external load. Consequently, only the results of embankment models resting on soft soil treated by end bearing ordinary stone columns are compared with analytical predictions.

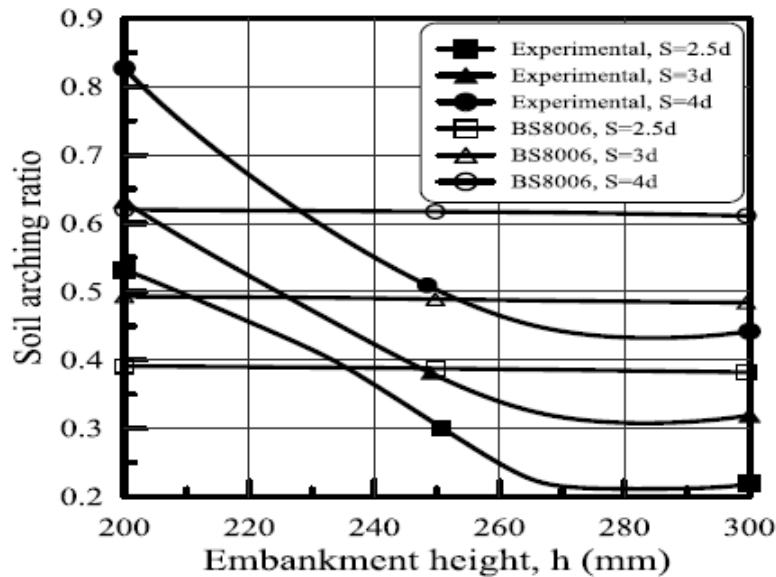


Fig. 25 Comparison between the test results and BS8006 design method for soil arching ratio

Fig. 23 shows that Terzaghi (1943) method always over predicts the soil arching ratio. However, at low embankment height and small spacing between columns, the results of this method shows good agreement with the minimum soil arching ratio from model tests.

The method of Hewlett and Randolph (1988) gives slightly lower results compared to experimental values for $h=200$ mm. This is attributed to the limit analysis of soil element assumed in the arch. The results of Hewlett and Randolph method are by far the most relevant when compared to experimental results for $h=250$ mm and 300 mm as shown in Fig. 24.

Marston's formula is applied to estimate the load on the pile cap in the British Standard BS8006 (1995). Moreover, the embankment fill material properties are not considered. As a whole, the soil arching ratio is strongly underestimated by BS8006 and constant for each spacing ratio when compared to the test results for end bearing columns ($L/d=8$) and floating columns ($L/d=5$) as shown in Fig. 25.

23. Conclusions

In this research, a series of 42 model tests performed on embankment models resting on soft clay treated with and without ordinary stone columns (OSC) and encased stone columns (ESC) have been undertaken to investigate the behavior of piled (stone columned) embankments. The study deals with the soil arching analysis of an embankment constructed on the reinforced soft soil with OSC and ESC. Parameters of study mainly considered variation of the embankment height (h), spacing ratio between stone columns (s/d) and length to diameter ratio of stone columns (L/d). Therefore, the most important findings from this research are summarized in the following points:

1. For OSC, when $(h/s-d) \leq 1.2$, there is virtually no effect of arching: 'ultimate' conditions are reached almost immediately, the settlement at the surface of the embankment is very large, and the stress acting on the subsoil is virtually unmodified from the nominal overburden stress.

2. As $(h/s-d)$ increases to 2.2, the stress on the subsoil does not increase significantly (and thus there is significant evidence of arching), and surface settlement reduced to lower values. It has been demonstrated that the critical value of $(h/s-d \approx 2.2)$ corresponds for full arching reported in this work.

3. For a high embankment, the stress state is not significantly affected above a height of 2.2 $(s-d)$.

4. Critical heights range between 1.2 $(s-d)$ to 2.2 $(s-d)$ from experimental data of stone-columned embankment compared with data from literature of piled embankment, good agreement with the value suggested by Terzaghi (1943) and with the ranges presented by Hewlett and Randolph (1988), Naughton (2007).

5. The Stress concentration ratio for embankment models treated by OSC and ESC is affected by the height of embankment, spacing between stone columns and L/d ratio. The value of (n) for models treated by ESC with $(s=2.5d)$ is higher than OSC at the same spacing and tending to be constant beyond $h=300$ mm for the two L/d ratios.

6. The ratio $h/(s-a)$ has been considered as an important parameter for arching behavior in design of piled (stone columned) embankment.

References

- Al-Shaikhly, A.A. (2000), "Effect of stone grain size on the behavior of stone column", M.Sc. Thesis, Building and Construction Engineering Department, University of Technology, Iraq.
- ASTM, D422 (2003), "Standard test method for particle-size analysis of soils", *Soil and Rock*, 04.08.
- ASTM, D854 (2003), "Standard test method for specific gravity of soil solids by water pycnometer", *Soil and Rock*, 04.08.
- ASTM, D4318 (2003), "Standard test method for liquid limit, plastic limit, and plasticity index of soils", *Soil and Rock*, 04.08.
- ASTM, D6637 (2003), "Standard test methods for determining tensile properties of geogrids by the single or multi-rib tensile method1", *Soil and Rock*, 04.08.
- British Standard B.S.:1377 part 2 (1990), "Methods of test for soils for civil engineering purposes general requirements and sample preparation", British Standard Institution, London.
- Britton, E. and Naughton, P. (2008), "An experimental investigation of arching in piled Embankments", *Proceedings of the 4th European Geosynthetics Conference*, Edinburgh, UK, September.
- Chen, R.P., Chen, Y.M., Han, J. and Xu, Z.Z. (2008), "A theoretical solution for pile-supported Embankments on soft soils under one-dimensional compression", *Can. Geotech. J.*, **45**(5), 611-623.
- Fattah, M.Y., Shlash, K.T. and Al-Waily, M.J. (2011), "Stress concentration ratio of model stone columns in soft clays", *Geotech. Test. J.*, **34**(1), 61-71.
- Fattah, M.Y. and Majeed, Q.G. (2012), "Finite element analysis of geogrid encased stone columns", *Geotech. Geolog. Eng. J.*, **30**, 713-726.
- Han, J. and Gabr, M.A. (2002), "Numerical analysis of geosynthetic reinforced and pile-supported earth platforms over soft soil", *J. Geotech. Geoenviron. Eng.*, **128**(1), 44-53.
- Han, J. and Collin, J.G. (2005), "Geosynthetic support system over pile foundations", *Geotech. Eng. Spec. Pub.*, ASCE, **130**(142), 3949-3953.
- Hewlett, W.J. and Randolph, M.F. (1988), "Analysis of piled Embankments", *Ground Eng.*, **21**(3), 12-18.
- Iglesia, G.R., Einstein, H.H. and Whitman, R.V. (1999), "Determination of vertical loading on underground structures based on an arching evolution concept", *Proceedings 3rd National Conference on Geo-Engineering for Underground Facilities*, Illinois, United States.
- Jenck, O., Dias, D. and Kastner, R. (2006), "Two-dimensional physical modelling of soft ground improvement by vertical rigid piles", *6th International Conference on Physical Modelling in Geotechnics ICPMG*, 527-532.

- Naughton, P.J. (2007), "The significance of critical height in the design of piled Embankments", *Proceedings of Geo-Denver 2007*, Denver, Colorado.
- Terzaghi, K. (1943), *Theoretical Soil Mechanics*, John Wiley and Sons, New York.
- Van Eekelen, S.J.M. and Bezuijen, A. (2008), "Design of piled Embankments considering the basic starting points of the British Standard BS8006", *Proceedings of the 4th European Geosynthetics Conference*, Edinburgh, UK.
- Yan Z. (2009), "Numerical modeling of arching in piled embankments including the effects of reinforcement and subsoil", Ph.D. Thesis, University of Nottingham, U.K.
- Van Eekelen, S.J.M., Bezuijen, A., Lodder, H.J. and Van Tol, A.F. (2012a), "Model experiments on piled Embankments, Part I", *Geotext. Geomembran.*, **32**, 69-81.
- Van Eekelen, S.J.M. Bezuijen, A., Lodder, H.J. and van Tol, A.F. (2012b), "Model experiments on piled Embankments, Part II", *Geotext. Geomembran.*, **32**, 82-94.
- Zhuang, Y., Wang, K.Y. and Liu, H.L. (2014), "A simplified model to analyze the reinforced piled Embankments", *Geotext. Geomembran.*, **42**, 154-165.